European Journal of Pharmaceutics and Biopharmaceutics 196 (2024) 114207

Contents lists available at ScienceDirect

European Journal of Pharmaceutics and Biopharmaceutics

journal homepage: www.elsevier.com/locate/ejpb

Research paper

Comparative analysis of lipid Nanoparticle-Mediated delivery of CRISPR-Cas9 RNP versus mRNA/sgRNA for gene editing *in vitro* and *in vivo*

Johanna Walther [a], Deja Porenta [a,b], Danny Wilbie [a], Cornelis Seinen [d], Naomi Benne [b], Qiangbing Yang [c,d], Olivier Gerrit de Jong [a], Zhiyong Lei [c,d], Enrico Mastrobattista [a,*]

[a] Department of Pharmaceutics, Utrecht Institute for Pharmaceutical Sciences (UIPS), Utrecht University, Universiteitsweg 99 3584 CG, Utrecht, the Netherlands
[b] Department of Infectious Diseases and immunology, Faculty of Veterinary Medicine, Utrecht University, Yalelaan 1, 3584 CL, Utrecht, the Netherlands
[c] Department of Cardiology, Laboratory of Experimental Cardiology, University Medical Center Utrecht, Heidelberglaan 100, 3584 CX, Utrecht, the Netherlands
[d] CDL Research, University Medical Center Utrecht, Heidelberglaan 100, 3584 CX, Utrecht, the Netherlands

ARTICLE INFO

Keywords:
CRISPR-Cas9
Cargo format
Lipid nanoparticles
In vitro assays
Systemic administration
Single cell flow cytometry

ABSTRACT

The discovery that the bacterial defense mechanism, CRISPR-Cas9, can be reprogrammed as a gene editing tool has revolutionized the field of gene editing. CRISPR-Cas9 can introduce a double-strand break at a specific targeted site within the genome. Subsequent intracellular repair mechanisms repair the double strand break that can either lead to gene knock-out (via the non-homologous end-joining pathway) or specific gene correction in the presence of a DNA template via homology-directed repair. With the latter, pathological mutations can be cut out and repaired. Advances are being made to utilize CRISPR-Cas9 in patients by incorporating its components into non-viral delivery vehicles that will protect them from premature degradation and deliver them to the targeted tissues. Herein, CRISPR-Cas9 can be delivered in the form of three different cargos: plasmid DNA, RNA or a ribonucleoprotein complex (RNP). We and others have recently shown that Cas9 RNP can be efficiently formulated in lipid-nanoparticles (LNP) leading to functional delivery *in vitro*. In this study, we compared LNP encapsulating the mRNA Cas9, sgRNA and HDR template against LNP containing Cas9-RNP and HDR template. Former showed smaller particle sizes, better protection against degrading enzymes and higher gene editing efficiencies on both reporter HEK293T cells and HEPA 1–6 cells in *in vitro* assays. Both formulations were additionally tested in female Ai9 mice on biodistribution and gene editing efficiency after systemic administration. LNP delivering mRNA Cas9 were retained mainly in the liver, with LNP delivering Cas9-RNPs additionally found in the spleen and lungs. Finally, gene editing in mice could only be concluded for LNP delivering mRNA Cas9 and sgRNA. These LNPs resulted in 60 % gene knock-out in hepatocytes. Delivery of mRNA Cas9 as cargo format was thereby concluded to surpass Cas9-RNP for application of CRISPR-Cas9 for gene editing *in vitro* and *in vivo*.

1. Introduction

Gene therapy is medical technology that modifies or manipulates the expression of a gene for therapeutic use. The discovery of reprogramming Clustered Regularly Interspaced Short Palindromic Repeats (CRISPR) associated (Cas) endonuclease, such as Cas9, as a genome editing tool, will greatly benefit gene therapy. [1] The Cas9 endonuclease forms an active ribonucleoprotein complex (RNP) with a synthetic single-guide RNA (sgRNA) and introduces a double strand break in the genome complementary to the sgRNA. [2] Succeeding cellular DNA repair mechanisms may either lead to gene knock-out by inducing insertions and deletion mutations (indels) via non-homologous end-joining (NHEJ) or repair based on homologous template via homology-directed repair (HDR). [3] Especially the latter is promising for gene therapy as a pathological mutation can be corrected in this manner.

For therapeutic application the CRISPR-Cas9 components require an *in vivo* delivery vehicle that arrives at the targeted cell population and delivers the CRISPR-Cas9 components intracellularly. Different viral and non-viral vectors are being designed for CRISPR-Cas9. [4] Especially non-viral nanoparticles are of great interest due to their relative ease of manufacturing. Moreover, viral vectors face the additional challenge of limitation in cargo size. [5] Amongst non-viral vectors, lipid nanoparticles (LNP), which employ cationic or ionizable cationic lipids, serve as promising candidates for delivery of Cas9 gene editing tool. The

* Corresponding author.
E-mail address: e.mastrobattista@uu.nl (E. Mastrobattista).

https://doi.org/10.1016/j.ejpb.2024.114207
Received 18 August 2023; Received in revised form 21 January 2024; Accepted 31 January 2024
Available online 6 February 2024

benefits of including ionizable cationic lipids in LNP formulations, such as C12-200, are effective encapsulation of cargo via electrostatic interactions, enhanced *in vivo* circulation time and cellular uptake, and endosomal cargo release. [6–8] Therefore, LNPs have been optimized for delivery of negatively charged nucleic acids such as plasmid DNA and mRNA, but also for Cas9-RNP. [9–13].

Despite the low costs and stability of plasmid DNA, recent efforts focus on delivering the cargo formats Cas9 mRNA or Cas9 RNP via lipid nanoparticles to reduce the risk of genomic integration and to minimize the delayed onset of gene editing. [14] Unlike plasmid DNA, which requires access to the nucleus for transcription to occur, Cas9 mRNA only needs to be delivered to the cytosol. [15] The cargo format mRNA molecule of LNPs has been shown to trigger Toll-like receptor 4 responses and subsequent immune responses that can then override the translation of mRNA to functional protein. [16] However, advances in chemical modifications such as substitution with pseudouridine, N6-methyladenosine or inosine suppress innate immune responses, and 5′-cap and secondary structures at 3′-terminus improve the resistance to RNAses. [17,18] The first clinical trials with mRNA Cas9 are on-going and resulting in promising genome editing outcomes, for example NTLA-2001 from Intellia Therapeutics which resulted in 87 % gene knock-out of TTR after a single dose of 0.3 mg per kilogram NTLA-2001 in patients. [9] In the case of delivery of the mRNA Cas9 the sgRNA needs to additionally be packaged within the LNP. The sgRNA then needs to form the RNP complex intracellularly after translation of the protein to perform gene editing in the nucleus. [19] For direct availability of the RNP, on-going efforts focus on formulating LNPs incorporating the Cas9 RNP. [10,20] It has been reported that the direct delivery of RNP would result in less off-target events as the Cas9-RNP is short-lived. [21] Furthermore, the use of RNPs ensures protection of sgRNA from degradation and at the same time complexation with sgRNA keeps Cas9 in its functional confirmation. [22,23] However, despite the net-negative charge of the Cas9-RNP allowing electrostatic interactions with the lipids, the negative charge is not uniformly distributed over the RNP surface. [24] Additionally, RNP is a large molecule. These attributes can affect the encapsulation of protein and moreover impact the structure, size and charge of LNPs. Due to different cellular membrane permeabilities and thus altering ability to take up LNPs varying in structure, size and charge, LNPs delivering Cas9-RNP may not be deliverable to all types of cells. [25] Just as LNPs delivering mRNA have shown immune activation described above, preexisting immunity against the bacterial protein risk premature clearance or toxicity. [26,27] In both cases, mRNA Cas9 or Cas9-RNP, a DNA HDR template will need to be packed within the LNP additionally in case of a precise repair strategy based on HDR.

For a better understanding and comparison, delivery of mRNA Cas9 and Cas9-RNP together with an HDR template via LNPs were investigated in this study. The advantages and disadvantages of these two formulations were determined by analyzing the size, surface charge, and morphology. In vitro assays allowed the determination of the activation of inflammatory responses and activity of the LNPs on two different cell types. Furthermore, the LNPs were compared in biodistribution and genome editing efficiencies *in vivo*.

2. Material and methods

All reagents and chemicals were commercially obtained from Sigma Aldrich (Zwijndrecht, The Netherlands) unless otherwise specified. SpCas9 was produced in-house via the method described in previous publication. [10] To fluorescently label the SpCas9, Alexa Fluor 647-C2 maleimide (ThermoFisher Scientific, Landsmeer, The Netherlands) was incubated with SpCas9 in a 20:1 M ratio of dye to protein in Tris buffer pH 7.4 (20 mM Tris, 300 mM NaCl). After overnight incubation at 4 °C, the excess dye was removed by gravity column chromatography using a PD 10 desalting column. After addition of 10 % glycerol, the labelled proteins were frozen in liquid nitrogen and stored at −80 °C. 2′O-methyl and phosphorothioate modified sgRNA as well as the Cy5.5-labelled sgRNA and template DNA were bought from Sigma-Aldrich (Haverhill, United Kingdom) and were stored in RNAse-free Tris EDTA buffer pH 7.0 (ThermoFischer Scientific). CleanCap mRNA Cas9 (5moU) was acquired from TeBu Bio (Heerhugowaard, The Netherlands). This mRNA was then fluorescently labelled with Cy5 in-house with the Label IT Nucleic Acid Labelling Cy5 Kit from Mirus Bio (Oxford, United Kingdom) following the manufacturer's protocol. Additionally, mRNA Cas9-GFP was ordered from Horizon Discovery (Waterbeach, United Kingdom). Furthermore, 1,10-((2-(4-(2-((2-(bis(2-hydroxydodecyl)amino)ethyl)(2-hydroxydodecyl)amino)ethyl)piperazin-1-yl)ethyl)azanediyl)bis(dodecan-2-ol) (C12-200) was acquired from CordonPharma (Plankstadt, Germany), 1,2-dioleoyl-*sn*-glycero-3-phosphoethanolamine (DOPE) from Lipoid (Steinhausen, Switzerland), Cholesterol and 1,2-dimyristoyl-*rac*-glycero-3-methoxypolyethyleneglycol-2000 (PEG-DMG) from Sigma-Aldrich, and 1,2-dioleoyl-3-trimethylammonium-propane (DOTAP) from Merck (Darmstadt, Germany).

2.1. Synthesis of modified mRNA Cas9

The production of modified mRNA was adapted from Warren et al. [28] Briefly, Cas9 plasmid served as template for PCR to prepare the IVT template. Forward primer used in the PCR was:

5′-TAATACGACTCACTATAAGGAAATAAGAGAGAAAAG −3′.

and reverse primer used to introduce 120 polyA tail sequence is:

5′-CTTCCTACTCAGGCTTTATTCAAAGACCA(T)120-3′.

These primers were synthesized by Integrated DNA Technologies (Leuven, Belgium). Reverse primer was synthesized as Ultramer oligos at a 4 nmol scale.

The modified mRNA was synthesized with slight modifications as described by Kogut et al. [29] For each 50 µl reaction of the VENI all-in-one mRNA Synthesis Kit with cap1 Analog (Leish Bio, Utrecht, The Netherlands), 2 µg of purified tail PCR product was provided as template. The final nucleotide concentrations in the reaction were 6 mM for the cap1 analog and 7.5 mM for adenosine triphosphate, guanosine triphosphate, cytidine triphosphate and N1-methylpseudouridine triphosphate. The RNA synthesis reaction was incubated at 37 °C for 30 min as instructed by the manufacturer. Subsequently, the RNA was purified through LiCL precipitation, dissolved in nuclease-free water, and quantified using Nanodrop (ThermoFisher Scientific). The purified RNA was stored at −20 °C until further use.

2.2. Formulation of lipid nanoparticles

Cas9-RNP LNPs co-delivering an HDR template (called *p*LNP-HDR for the rest of the manuscript) were formulated as described in a previous publication. [10] In short, Cas9 and sgRNA were mixed together at a 1:1 M ratio (1.6 µM sgRNA) to formulate the ribonucleoprotein complex in nuclease-free water. After 15 min, an ssODN HDR template was added at a 2:1 M ratio to the RNP. The CRISPR-Cas9 components were then mixed by pipette-mixing with the lipids at a volume ratio of 3:1 and weight ratio 40:1 (total lipids to sgRNA). The lipid composition is C12-200, DOPE, cholesterol, PEG-DMG, DOTAP with molar ratios of 35:16:46.5:2.5:0.25, respectively. Lipids are resuspended in ethanol. To formulate mRNA Cas9 formulations (named *m*LNP-HDR), the same lipid composition and ratio to sgRNA concentration was used. HDR template concentration was also kept the same. However, as described in literature, mRNA Cas9 was added at a 4:1 wt ratio to the sgRNA. [20] Weight mass of each component of the formulations can be found in supplementary table 4.

LNPs used in the animal studies were made with the same properties but at higher concentrations (RNP = 15 µM). mRNA Cas9 used for the formulations for *in vivo* was synthesized as described above. These LNP were made without an HDR template, but only encapsulate the Cas9-RNP (named *p*LNP) or Cas9 mRNA and sgRNA (name *m*LNP). Additionally, the formulations were dialyzed against 1x PBS overnight with

Float-A-Lyzer molecular weight cut-off (MWCO) 300 kDA dialysis chambers (Avantor®, Arnhem, The Netherlands).

All sequences of sgRNA and HDR template used in this study are given in Supplementary Table 1.

2.3. Physical characterizations of the Cas9-RNP and mRNA LNPs

The average size and polydispersity index (PDI) of the lipid nanoparticle formulations were determined after a 1.3-fold dilution in 1 X PBS (pH 7.4) by dynamic light scattering using a Zetasizer Nano S (Malvern ALV CGS-3, Malvern, United Kingdom). The Zetasizer Nano Z (Malvern ALV CGS-3, Malvern, United Kingdom) was used to determine the ζ-potential, whereby the formulations had prior to measurements been diluted 9-fold in 10 mM HEPES buffer at pH 7.4.

2.4. Gel assays

Fluorescently-labelled CRISPR-Cas9 components (Alexa647-SpCas9, Cy5-mRNA Cas9, ATT550-sgRNA, 6-FAM-HDR-template) were complexed with lipids as described above to obtain a Cas9-RNP and an mRNA formulation. Then, 40 % glycerol was added to the LNPs to reach a final concentration of 10 % glycerol (1:5 v/v). Twenty microliters of the glycerol-treated samples were loaded onto a 2 % agarose gel and run at 100 V for 30 min in 1 x TAE buffer pH 8 (BioRad Laboratories B.V, Veenendaal, The Netherlands). The gel was then imaged with ChemiDoc Imaging System (Bio-Rad Laboratories B.V) using the channels (Cy5 (protein and mRNA), Alexa488 (HDR template), Alexa467 (sgRNA) to depict the fluorescent signals.

An enzymatic degradation study was performed to determine the degree of protection of the CRISPR-Cas9 components by the LNPs. LNP formulations incorporating Alexa647-labelled Cas9-RNP were treated with different v/v percentages of trypsin (0, 1, 5, 10, 20, 50 %) and Cy5-labelled mRNA formulations were treated with RNase A (at same percentages). *m*LNPs and *p*LNPs were treated with trypsin or RNAse for 30 min at 37 °C, respectively. To determine the degree of protection of the CRISPR-Cas9 components provided by the LNP complexation against trypsin and RNase degradation, Alexa647-labelled Cas9-RNP and Cy5-labelled mRNA formulations were treated with different percentages of trypsin and RNase (0, 1, 5, 10, 20, 50 %), respectively, for 30 min at 37 °C. Twenty microliters of the glycerol-treated samples were loaded onto a 2 % agarose gel and run at 100 V for 30 min. The gel was then imaged with a ChemiDoc Imaging System (Bio-Rad Laboratories B.V) using the Cy5 channel. The percentage of degradation was quantified by determining the intensity of the gel bands by densitometry in ImageJ (version 1.52p).

Table 1
Antibody staining of parenchymal and non-parenchymal liver cells. For more information about the antibodies see supplementary table 2. As indicated in the table, laser 561 paired with filter 585–42 was used for the detection of PE-labelled MHC-II antibody or tdTomato *in vivo*. Laser 637 paired with filter 712–25 was either used for detection of Cy5.5 fluorescence (biodistribution study) or Alexa700-labelled MHC-II (functionality study).

Laser	Filter	Fluorophore	Marker	Dilution of antibody
405	450–45 (405)	**eFluor 450**	CD11b	1:800
	525–40 (405)	**BV510**	CD31	1:200
			B220	1:200
488	525–40 (488)	**Alexa488**	CD45	1:400
561	585–42 (561)	**PE (biodistribution) or tdTomato**	MHC-II (biodistribution) or gene editing	1:800
	763–43 (561)	**PE-Vio770**	CD11c	1:400
637	660–10 (637)	**APC**	F4/80	1:200
	712–25 (637)	**Cy5.5 or Alexa700 (functionality)**	LNP or MHC-II (functionality)	1:400
808	885–40 (808)	**Viakrome**	Live/dead	1:1000

2.5. Imaging of LNPs with cryo-TEM

Ten microliter of nanoparticles in suspension in 1x PBS were added to freshly glow-discharged quantifoils and incubated for at least 10 min in a humidified environment. Then, the samples were vitrified using a FEI Mark IV Vitrobot (Fei, Hillsboro OR, USA) and subsequently stored in liquid nitrogen until imaging. Samples were imaged on a FEI Tecnai G2 20 TWIN 200 kV transmission electron microscope whereby vitrified quantifoils were loaded in a Gatan 70° tilt cryo-transfer system (pre-cooled using liquid nitrogen) and inserted in the microscope. Samples were imaged at a magnification of 29 k and images were acquired by the bottom-mounted FEI High-Sensitive (HS) 4 k x 4 k Eagle CCD Camera System.

2.6. Generation of eGFP HEPA 1–6

Hepa 1–6 cells were kindly gifted to us from dr. Piter Bosma (Tytgat Institute for Liver and Intestinal Research, Amsterdam University Medical Center). To produce hepatocyte cells stably expressing eGFP, lentivirus vectors encoding for eGFP and antibiotic-resistance towards puromycin were used for lentiviral production. Firstly, HEK293T cells (ATCC, Molsheim Cedex, France) were passaged to ensure a 30–50 % confluency on the following day in a T25 cell culture flask. After obtaining 30–50 % confluency, the HEK293T cells were transfected with a mixture of 2 μg PSPAx2, 2 μg pMD2.G-G, and 4 μg lentiviral transfer plasmid (pHAGE2-EF1a-eGFP-IRES-PuroR-WPRE) in OptiMEM using 3 μg PEI per μg DNA and incubated at 37 °C and 5 % CO_2 overnight. The medium was refreshed with 5.5 ml DMEM medium supplemented with 10 % FBS (S1810-500, Biowest, VWR International, Amsterdam, The Netherlands) and 1 % antimycotic/antibiotic solution and placed back into the cell incubator for 48 h. Then, the conditioned medium was harvested from the HEK293T cells into a 15 ml falcon tube and centrifuged at 500 x g for 5 min. The supernatant was isolated and filtered through a 0.45 μm RC membrane filter (Phenomenex, Utrecht, The Netherlands). Directly afterwards, HEPA1-6 cells were treated with the filtered solution containing the lentivirus for production of eGFP-positive HEPA1-6 cells and incubated at 37 °C and 5 % CO_2 for 3 days. Subsequently, the cells were selected for eGFP-positive cells via antibiotic selection with 2 μg/ml puromycin. During the following 3 weeks the cells were cultured under selection pressure through puromycin (InvivoGen, Toulouse, France). Subsequently, the cells were sorted using a BD FACSAria III cell sorter and afterwards continuously expanded in the presence of selection antibiotic puromycin.

2.7. Cell culture

eGFP HEK293T cells were cultured at 37 °C and 5 % CO_2 in DMEM low glucose (Sigma, Merck Life Science NV, Amsterdam, The Netherlands) supplemented with 10 % FBS (S1810-500, Biowest) and 1 mg/ml geneticin (G418 sulfate, ThermoFischer Scientific). [10] eGFP HEPA1-6 cells were cultured at same culture conditions however with DMEM high glucose (Sigma, Merck Life Science NV) supplemented with 10 % FBS and 2 μg/ml puromycin. HEK293T cells and HEK293T HDR Stoplight cells were cultured in DMEM low glucose medium supplemented with 10 % FBS. [30].

2.8. Gene editing efficiency assay on eGFP HEK293T and eGFP hepa1-6 cells

eGFP HEK293T cells and eGFP HEPA1-6 cells were plated with a cell density of 10,000 cells/well onto a clear F-bottom 96-well plate and then incubated at 37 °C and 5 % CO_2. The following day, the medium was supplemented with antibiotic/antimycotic solution. *p*LNP-HDR or *m*LNP-HDR (using sgGFP and HDR template for GFP -> BFP conversion) were then added to wells in duplicates in different concentrations and the cells were then incubated again for two days at 37 °C and 5 % CO_2. [31] Cells were passaged and expanded onto 12 well plates for an additional two days and then harvested, washed twice and fixed in 1 % paraformaldehyde. Cells were transferred to a BD Falcon U-bottom 96-well plate (Becton Dickinson, Franklin Lakes, NJ, USA) for detection of fluorescent signal by flow cytometry using the BD FACS CANTO II (Becton Dickinson). BFP signal was excited by laser with 405 nm wavelength and picked up by filter 450/50 (laser 405 nm) and eGFP fluorescence was excited by laser with wavelength 488 nm and detected in filter 530/30. Data was then analyzed with the Flowlogic software (version 8.6, Inivai Technologies, Mentone, Australia). Cell populations classified as gene knock-out are eGFP negative and BFP negative and cell populations classified as gene correction are eGFP negative and BFP positive. [10].

The experiment was repeated three individual times, whereby in one experiment a positive control was additionally added. ProDeliverIN CRISPR (Oz Biosciences, San Diego, California) was used to deliver the RNP and HDR template in a molar ratio of 15:15:28.5 nM (Cas9:sgRNA:HDR).

2.9. Uptake of eGFP-*Cas9* RNP vs eGFP-Cas9 mRNA LNPs in HEK293T cells

HEK293T cells were plated at a cell density of 10,000 cells/well on a flat bottom black 96-well plate and then incubated at 37 °C and 5 % CO_2 overnight. Ten microliters (sgRNA concentration = 15 nM) of either eCas9-GFP RNP or eCas9-GFP mRNA LNPs were added to the wells at different timepoints. The wells were then treated collectively with the nuclei stain Hoechst 33,342 at a final concentration of 2 μg/ml in OptiMEM (Gibco TM, Fisher Scientific) for 10 min at 37 °C and 5 % CO_2. The cells were then imaged with confocal microscopy using the Yokogawa Cell Voyager 7000S (CV7000S) Confocal Microscope (Yokogawa Corporation, Tokyo, Japan). Signal intensities of GFP within the detected nuclei were determined with image analysis using the Columbus Software (Perkin Elmer, version 2.7.1). The analysis method can be found in supplementary figure 7.

2.10. Timing of gene correction on HEK293T HDR Stoplight cells HEK293T cells

To follow the onset of gene correction mediated through *p*LNP or *m*LNP, HEK293T HDR Stoplight cells were used. [30] These cells continuously express mCherry however, upon introduction of a double strand break downstream of the mCherry coding sequence and subsequent homology directed repair, a stop codon (TAA) is altered to Glutamine (GAA), resulting in eGFP expression.

The cells were plated at a density of 10,000 cells/well in low glucose DMEM medium supplemented with 10 % FBS on a flat bottom black 96-well plate (Greiner #955090) and incubated at 37 °C and 5 % CO_2. The following day, 10 μl (sgRNA concentration = 15 nM) of either *p*LNP-HDR or *m*LNP-HDR were added to the wells at different timepoints. After 48 h, all wells were washed by aspirating off the medium and treated with the nuclear stain Hoechst at a final concentration of 2 μg/ml in OptiMEM for 10 min at 37 °C and 5 % CO_2. Then, the cells were imaged with confocal microscopy using the Yokogawa CV7000S Confocal Microscope. Gene correction efficiencies (= # GFP positive cells/# mCherry positive cells) were determined by image analysis with Columbus Software (Perkin Elmer, version 2.7.1). The analysis method can be found in supplementary figure 8. Additionally, the mean fluorescent intensity of GFP was calculated for all cells of one microscopy image.

2.11. Determination of cytokine production via qPCR

Bone marrow isolated from the femurs and tibias of WT BALB/c mice were homogenized and seeded in 6-well plates at a cell density of 450,000 cells/mL in 2 ml IMDM (Gibco, ThermoFisher Scientific, Landsmeer, The Netherlands) supplemented with 10 % FCS (Bodinco, Alkmaar, The Netherlands), 100 units/mL of penicillin (Gibco, ThermoFisher Scientific), 100 ug/mL of streptomycin (Gibco, ThermoFisher Scientific) and 0.5 μM β-mercaptoethanol (Gibco, ThermoFisher Scientific). To induce DC differentiation, 20 ng/mL of granulocyte–macrophage colony-stimulating factor (GM-CSF, in-house produced) was added. Cells were cultured at 37 °C and 5 % CO_2 for a total of 6 days. After 2 days, 2 ml of IMDM and 20 ng/mL GM-CSF were added to the wells. On day 5 GM-CSF (20 ng/mL) was added. On day 6, cells were harvested by scraping. For qPCR cells were plated out at 900,000 cells/well in an F-bottom 12-well plate. The cells were left to adhere for 2 h. Cells were stimulated with different concentrations pLNP-HDR and mLNP-HDR based on sgRNA molar concentration (30, 15, 7.5 nM). As controls, immature DCs (iDCs) were unstimulated, and mature DCs (mDCs) were stimulated with 10 ng/mL LPS (O111:B4; Sigma-Aldrich). After 24 h, supernatants were carefully removed, and cells were lysed with RLT buffer (Qiagen Benelux B.V., Venlo, the Netherlands). Total mRNA was immediately extracted using the RNeasy kit (Qiagen) according to the manufacturer's instructions. Transcription of mRNA into cDNA was performed using the iScript™ cDNA Synthesis Kit (Bio-Rad Laboratories B.V.) according to manufacturers' instructions. PCR and Real-Time detection were performed using a Bio-Rad MyiQ iCycler (Bio-Rad). Amplification was performed using IQ™ SYBR Green® Supermix (Bio-Rad) with 0.25 μM final concentrations of primer sets for *IL10* (5′-GGT TGC CAA GCC TTA TCG GA-3′ and 5′-ACC TGC TCC ACT GCC TTG CT-3′), *IL12B* (5′-GGA AGC ACG GCA GCA GAA TA-3′ and 5′-AAC TTG AGG GAG AAG TAG GAA TGG-3′), *TNF* (5′-CCC TCA CAC TCA GAT CAT CTT CT-3′ and 5′-GCT ACG ACG TGG GCT ACA G-3′), *IFNA1* (5′-TAC TCA GCA GAC CTT GAA CCT-3′ and 5′-CAG TCT TGG CAG CAA GTT GAC-3′), *TRAF6* (5′-AAA GCG AGA GAT TCT TTC CCT G-3′ and 5′-ACT GGG GAC AAT TCA CTA GAG C-3′), and *HPRT* (5′-CTG GTG AAA AGG ACC TCT CG-3′ and 5′-TGA AGT ACT CAT TAT AGT CAA GGG CA-3′). The qPCR was performed for 40 cycles using the following settings: denaturation at 95 °C for 20 sec, annealing at 59 °C for 30 sec. mRNA expression within each sample was normalized to the detected C_t value of *HPRT* and expressed relative to the average C_t value of the mDC control.

2.12. Animal studies

Twenty-four female Ai9 mice (B6.Cg-Gt (ROSA) 26Sor tm9 (CAG-tdTomato) Hze/J) were bred at PSP Bilthoven (Bilthoven, The Netherlands) and were 8–12 weeks old at the start of the animal study. Animals were kept under standard conditions of the animal facility (standard chow and water *ad libitum*) and all experiments were approved by the Animal Experiment Committee of Utrecht University and complied with the Dutch Experiments on Animals Act (WOD) under the license AVD10800202115026.

The animal study was split into two parts: 1.) Biodistribution of Cy5.5-labelled sgRNA targeting a stop codon prior to the tdTomato gene construct (Cy5.5-sgTOM) delivered via *p*LNP or *m*LNP in comparison to a non-targeting unlabelled sgRNA targeting nucleotides 200–219 in the eGFP construct (sgGFP) in *p*LNP (see supplementary information table 1 and 2.). Functionality of gene knock-out resulting in tdTomato expression after IV injections of *p*LNP and *m*LNP (both formulations without HDR template). Each experimental group for each part had four mice per

group.

Biodistribution

Mice were administered with LNP encapsulating RNP (5 % Cy5.5-sgTOM) or mRNA and sgTOM (5 % Cy5.5-sgTOM) at a dose of 20 μg of sgRNA in total, respectively, by tail vein injections. The mice of the control group were administered with LNP encapsulating RNP (unlabelled sgGFP) at the same dose of total sgRNA as the two other experimental groups. After 4 h, mice were anesthetized with 0.1 mg/kg fentanyl, 10 mg/kg midazolam and 1 mg/kg medetomidine via IP injection. Then, mice were perfused with PBS via the left ventricle cavity. Liver, kidney, lungs, spleen, heart, ovaries, and brain were harvested for further analysis.

Functionality of gene knock-out.

Mice of all three experimental groups (*p*LNP, *m*LNP, and non-targeting *p*LNP) were injected with LNPs at a dose of 20 μg sgTOM via tail vein injections. Seven days later, mice were anesthetized with 0.1 mg/kg fentanyl, 10 mg/kg midazolam and 1 mg/kg medetomidine via IP injection and then perfused with PBS. Liver, kidney, lungs, spleen, heart, ovaries and brain were collected for further analysis.

2.13. Biodistribution of Cy5.5-labelled sgRNA delivered via LNP RNP or LNP mRNA Cas9 & sgRNA

Harvested organs of mice administered with LNPs as described above were imaged with a Pearl Impulse Imager (LI-COR Biosciences) using channels 700 nm, 800 nm, and white to trace back Cy5.5-labelled sgRNA. All images were further analyzed by Image Studio Lite Software (LI-Cor Biosciences). To quantify the fluorescent signal a region of interest was drawn manually around the separate organs and the total fluorescent intensity was divided by the weight of the imaged organ.

2.14. Single cell flow cytometry

One third of the harvested liver was further processed for single cell flow cytometry. The tissue was submerged in 5 ml prewarmed digestion buffer (RPMI-1640 medium supplemented with 1 mg/ml type IV collagenase A (Sigma-Aldrich, Cat. No. C5138)) and minced with surgical blades. The minced tissue was then transferred to a 50 ml falcon tube and another 10 ml of digestion buffer was added and incubated at 37 °C for 30 min while gently swirling the mixture every 5 min. Then, the digested cell suspension was strained through a nylon cell strainer (ThermoFisher Scientific). The strained suspension was centrifuged at 70g for 2 min to separate the parenchymal and non-parenchymal cells. The supernatant containing the non-parenchymal cells was transferred to a new tube and centrifuged at 500g for 7 min at 4 °C and the supernatant was then removed. The cell pellet was resuspended in 2 ml ACK lysis buffer (Gibco, ThermoFisher Scientific) for 3 min, and then diluted with cold PBS. Cells were again centrifuged at 500g for 7 min at 4 °C. Meanwhile, the parenchymal cells were washed with 10 ml cold PBS and then centrifuged at 70g for 2 min at 4 °C. The cells were resuspended in 200 μl of RPMI-1640 medium and transferred to a 96-well V-bottom plate (ThermoFisher Scientific) and stored on ice until further processing. The pelleted non-parenchymal cells were resuspended in 1–5 ml RPMI-1640 medium and plated onto the V-bottom plate with a cell density of 300,000 cells/well. The plate was centrifuged at 175 x g for 5 min at 4 °C. Cells were resuspended in 25 μl of FcBlock (2.4G2 monoclonal antibody, produced by Department of Infectious Diseases and Immunology, Utrecht University) and incubated for 5 min at 4 °C. [32] Seventy-five microliter of antibody staining solution in FACS buffer (2 % FCS, 0.005 % NaN_3 in PBS) was added per well (see table 1 and supplementary table 2) and the stained plate was incubated in the dark for 30 min. Cells were washed with PBS three times and then resuspended in 100 μl of FACS buffer and measured on the CytoFlex LX flow cytometer. Data was processed and analyzed in FlowLogic and the gating strategy is shown in Supplementary Fig. 11.

3. Results

3.1. Physical characterization of lipid nanoparticles encapsulating pLNP-HDR and mLNP-HDR

Nanoparticles were formulated as described in previous publication in the presence of 0.25 mol% DOTAP to mediate electrostatic interactions between lipid and cargo in nuclease-free water. [10] The characterization of the formulations encapsulating Cas9-mRNA (named *m*LNP-HDR) or Cas9-RNP (named *p*LNP-HDR) was performed as described. *m*LNP-HDR are smaller in their average size and more monodisperse than *p*LNP-HDR (150 nm vs 245 nm and PDI 0.12 vs 0.26, respectively) as shown in Fig. 1A. Cryo-TEM images displayed in Fig. 1B show that both *p*LNP-HDR and *m*LNP-HDR take the shape of lipoplexes and spheres. *p*LNP and *m*LNP without HDR templates were additionally characterized as spherical particles via cryo-TEM (see Supplementary Fig. 1). Within the cryo-TEM images of *p*LNP-HDR, however, more dense structures were observed compared to *m*LNP-HDR (Fig. 1B, middle). Gel retardation assays with fluorescently-labelled CRISPR-Cas9 components showed that Cas9-RNP and HDR template and Cas9-mRNA, sgRNA, and HDR template remain retained within *p*LNP-HDR and *m*LNP-HDR, respectively (Fig. 2C). Some non-complexed HDR template was detected in both *p*LNP-HDR and *m*LNP-HDR (Fig. 2C lane 1,2). The lipid nanoparticles provide protection against trypsin, an endopeptidase, and RNAse indicating that the Cas9 protein or mRNA are incorporated in a lipid core (Fig. 2D,E). At higher percentages of trypsin, Cas9 eventually does degrade and degradation was quantified to a percentage of 20 % after 30 min incubation with 50 % trypsin as can be seen in Supplementary Fig. 3.

3.2. Timing of gene editing and gene editing efficiencies of pLNP and mRNA in vitro

After physical characterization, *p*LNP-HDR and *m*LNP-HDR were compared in terms of kinetics of gene correction and gene editing efficiencies on eGFP reporter cell lines in culture. Delivery of the CRISPR-Cas9 components as RNP or mRNA via *p*LNP-HDR and *m*LNP-HDR, respectively, resulted in gene editing efficiencies comparable or higher to the commercial transfection agent ProDeliverIN CRISPR (Fig. 2A). *m*LNP-HDR however resulted in about a 5-fold higher efficiency than *p*LNP: 80 % gene knock-out and 15 % gene correction at 30 nM sgGFP versus to 24 % gene knock-out and 5 % gene correction via *p*LNP-HDR (Fig. 2A). Interestingly, gene editing efficiencies of eGFP construct were higher in HEK293T cells than in hepatoma cells, wherein especially gene correction did not exceed over 2 % for *p*LNP-HDR nor for *m*LNP-HDR (Fig. 2A). *m*LNP-HDR resulted in saturation of gene knock-out on eGFP HEK293T cells already at a final concentration of 3.8 nM sgGFP. The relative gene corrections (determined as fraction of total edits), however, were similar between the two different formulations on eGFP HEK293T cells, but higher for *p*LNP-HDR on eGFP HEPA1-6 cells as shown in Fig. 2B.

Cellular toxicity assays shown in supplementary figure 4C indicate that *p*LNP-HDR show higher cytotoxicity with eGFP HEK293T cells than *m*LNP-HDR, while both *p*LNP-HDR and *m*LNP-HDR do not result in toxicity on eGFP HEPA1-6 cells. Over time, both formulations lose functionality, but do not change in size (Supplementary Fig. 4A,B). However, notably, *p*LNP-HDR aggregated and sedimented over time (Supplementary Fig. 5).

To gain insight in the timing of delivery of Cas9 protein to the cytosol and subsequently the nucleus, the presence of eGFP-Cas9 fusion protein was measured by fluorescence confocal microscopy in HEK293T cells. Cas9 protein was located within the cytosol and nucleus within 30 min after transfection of cells with *p*LNP-HDR (Fig. 2C). When delivered as mRNA, eGFP-Cas9 fusion protein was first detected in the cytosol and nucleus after 4 h (2C). Furthermore, it is interesting to highlight that the eGFP-Cas9 fusion protein signal within HEK293T cells differs in

A

formulation	lipid compounds	cargo	size	PDI	ζ-potential
pLNP-HDR	C12-200, DOPE, cholesterol, PEG-DMG, DOTAP	Cas9-RNP, HDR template	245 ± 4 nm	0.26 ± 0.01	-10.8 ± 0.8 mV
mLNP-HDR	C12-200, DOPE, cholesterol, PEG-DMG, DOTAP	Cas9 mRNA, sgRNA, HDR template	150 ± 2 nm	0.12 ± 0.03	-12.4 ± 1.5 mV

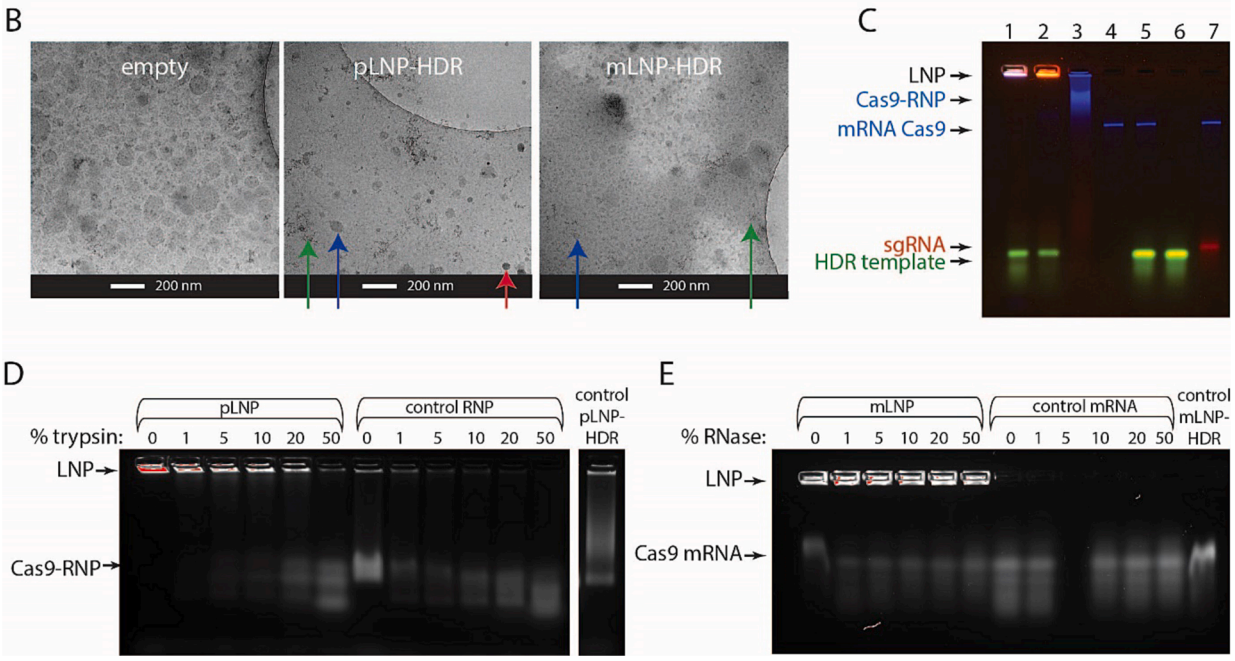

Fig. 1. Physical characterizations of *p*LNP-HDR and *m*LNP-HDR. A) Overview of the formulation's lipid compounds, cargo, size, polydispersity index (PDI) and charge. **B)** Cryo-TEM images of empty LNPs and *p*LNP-HDR and *m*LNP-HDR. Scale bar represents 200 nm. Green arrows indicate lipoplex structures, blue arrows point to spherical particles, and red arrows indicate dense particles. **C)** Gel retardation assay of labelled CRISPR-Cas9 components for determination of entrapment of cargo in LNPs. SpCas9 – Alexa647 (blue), mRNA – Cy5 (blue), sgRNA – ATTO550 (red), HDR template – 6FAM (green). Gel lanes: 1 – pLNP, 2 – mLNP, 3 – control Cas9-RNP, 4 – control mRNA Cas9, 5 – control mRNA Cas9 & HDR template, 6 – control HDR template, 7 – control mRNA Cas9 & sgRNA. Pink indicates overlap of mainly blue (Cas9) and red (sgRNA) signal but also green (HDR template). Orange color indicates overlap of blue (mRNA Cas9), red (sgRNA), and green (HDR template). **D)** Agarose gel of a trypzination assay to determine protection and localization of Alexa647-Cas9-RNP in *p*LNP-HDR. Control *p*LNP-HDR (from a separate gel) was treated with final concentration of 2 % triton to disrupt lipids. The lowest band on the gel was assigned for calculation of percentage of degradation via trypsin as shown in Supplementary Fig. 3. **E)** Agarose gel of an RNAse assay to determine protection and localization of Cy5-mRNA Cas9 in *m*LNP-HDR. Control *m*LNP-HDR was treated with final concentration of 2 % triton to disrupt lipids. (For interpretation of the references to color in this figure legend, the reader is referred to the web version of this article.)

intensity between *p*LNP and *m*LNP-mediated delivery (images shown in Supplementary Fig. 6).. Despite the earlier delivery of Cas9 in the nucleus via *p*LNP, gene correction became apparent after 22 h in HEK293T HDR Stoplight cells, reporter cells in which gene correction results in a GFP signal (Fig. 2D), treated with *m*LNP-HDR (Fig. 2E) and saturating after 30 h. Onset of gene correction detected in the cells treated with *p*LNP-HDR occurred around 24 h but was determined to still increase until the end of the experiment (48 h).

LNPs encapsulating Cas9-RNP or mRNA Cas9 were compared on stimulation of inflammatory cytokines after treatment of DCs with LNPs via qPCR. *m*LNP-HDR triggered 13-fold higher expression of IFN-α to mDCs while *p*LNP-HDR resulted in a 5-fold expression at 30 nM sgRNA (Fig. 2F). Cytokines TRAF6 and TNF-α were only expressed 3-fold and 5-fold, respectively, higher than mDCs after treatment with *p*LNP-HDR, while *m*LNP-HDR upregulated expression of IL-12 and IL-10.

3.3. *In vivo* biodistribution and gene knock-out efficiencies of pLNP RNP and mLNP

After *in vitro* characterization, the *p*LNP and *m*LNP formulations were compared in biodistribution and gene editing functionality, specifically gene knock-out, in female Ai9 mice as shown in the schematic representation in Fig. 3A. Both formulations were larger in particle size with a higher PDI at these concentrations than the formulations for *in vitro* work described above (Supplementary Fig. 10B). Four hours after administration intravenously, *p*LNP were detected in the liver, spleen and lungs while Cy5.5-sgTOM via *m*LNP was detected in the liver, lungs, and kidneys (Fig. 3B,C,D). The biodistribution study had been split into two separate runs. In the first run, the signal of Cy5.5 + -sgTOM via *p*LNP was higher in the lungs than in the second run (Supplementary Fig. 13). Notably, in general the fluorescent signal of Cy5.5-sgTOM is stronger in organs of mice treated with *p*LNP. On closer look at the liver, Fig. 3E shows that Cy5.5-sgTOM delivered via *p*LNP was mainly detected in liver sinusoidal endothelial cells (LSEC) (71 % of cells positive for Cy5.5 signal) and additionally in dendritic cells (14 %) and hepatocytes (12 %). Cy5.5-sgTOM delivered by *m*LNP also resulted in uptake mainly in LSEC (46 %), and in dendritic cells (13 %) and hepatocytes (41 %). One mouse that received control formulation (*p*LNP with irrelevant sgRNA) within the biodistribution study died after IV injection. To investigate the gene knock-out efficiency of the stop codon resulting in

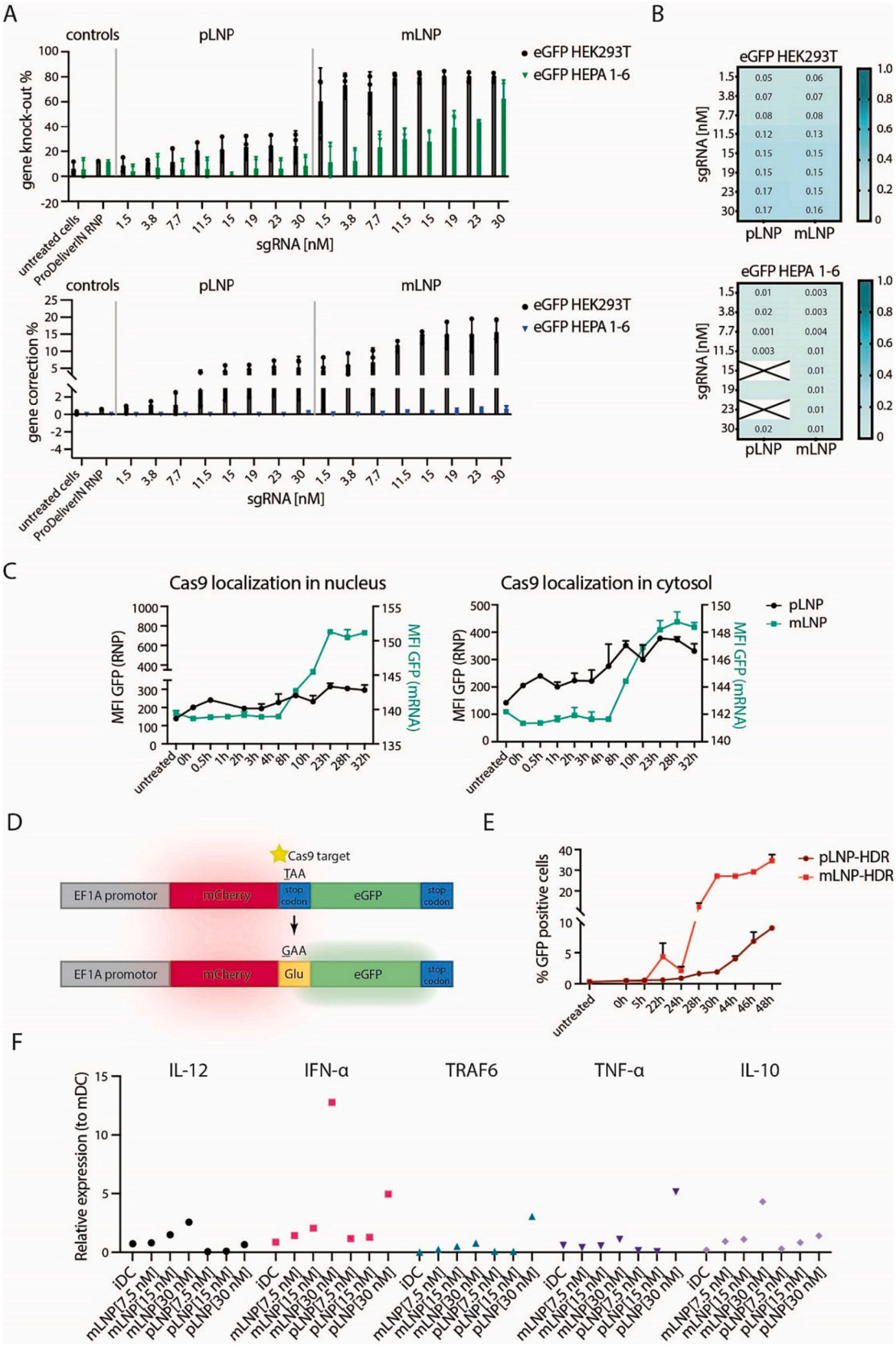

(caption on next page)

Fig. 2. Comparison of *p*LNP and *m*LNP on intracellular delivery of Cas9, gene editing efficiency and timing of HDR on-set. A) Gene knock-out (top) of eGFP fluorescence and gene correction (bottom) of eGFP to BFP fluorescence in eGFP HEK293T and eGFP HEPA1-6 cells mediated through different concentrations of *p*LNP and *m*LNP (n = 3). sgGFP and HDR template for GFP reporter system used in this experiment (see supplementary table 1). **B)** Heatmaps of relative gene correction between *p*LNP and *m*LNP in eGFP HEK293T (top) and eGFP HEPA1-6 (bottom) cells. **C)** Uptake of eGFP-Cas9 fusion protein delivered as RNP or as mRNA via LNP in nucleus (left) and cytosol (right) of HEK293T cells over time. MFI of eGFP-Cas9 was determined by image analysis of confocal microscopy images with the Columbus software. **D)** Scheme of HEK293T HDR Stoplight cells: gene editing of a stop codon (TAA->GAA) via HDR results in expression of eGFP. **E)** Onset of homology-directed repair in HEK293T HDR Stoplight cells. Percentage of GFP positive cells was determined as GFP positive cells within mCherry positive cells by image analysis of confocal microscopy images with the Columbus software. sgSTOP and HDR template for HDR Stoplight system were used in this experiment. **F)** Expression of cytokines (IL-10, IFN-α, TRAF6, TNF-α, IL-10) relative to LPS-stimulated matured mature dendritic cells (expression of 1) of dendritic cells treated with *p*LNP-HDR or *m*LNP-HDR measured via qPCR. Immature dendritic cells (iDCs) are plotted as control values.

the expression of tdTomato, female Ai9 mice were injected intravenously with *p*LNP and *m*LNP. Within 20 h all mice treated with *p*LNP died and only *m*LNP-treated mice lived until the end of the experiment. Within the liver, *m*LNP were found to result in 60 % tdTomato-positive hepatocytes, hence successful gene knock-out (Fig. 3F). tdTomato-positive cells were not detected in LSEC, myeloid cells, Kupffer cells or dendritic cells.

4. Discussion

This study shows a comparison of lipid nanoparticles delivering CRISPR-Cas9 components either as single molecules, mRNA Cas9 and sgRNA, or directly as ribonucleoprotein complex. The formulation of *p*LNP-HDR was based on our previous publication. [10] The same formulation conditions were used for *m*LNP-HDR, except that mRNA Cas9 was added to sgRNA in a 4:1 wt ratio prior to complexation with lipids. *m*LNP-HDR were found to be more monodisperse (PDI 0.12) in their size (150 nm) than *p*LNP-HDR and additionally the lipids seem to protect the mRNA Cas9 more efficiently against higher concentrations of degrading enzymes (Fig. 1). From this result we conclude that mRNA Cas9 is better incorporated into the core of LNPs, while the Cas9-RNP is partially associated to the outside surface. While the Cas9-RNP has a net-negative charge, the distribution of anions has been shown to not be equally distributed across the surface of the RNP. [24] This might affect the incorporation of the Cas9-RNP into the core of LNPs, which can additionally explain the difference in size of particles. Nonetheless, gel retardation studies (Fig. 1C) showed that both *p*LNP-HDR and *m*LNP-HDR formulations retained the Cas9-RNP or mRNA Cas9 and sgRNA, respectively. HDR template was also retained in both formulations, though gel assay also showed uncomplexed HDR template. Additional studies, such as single-particle analysis by a dedicated flow cytometer, e.g. nanoFCM, should be performed to confirm that each CRISPR-Cas9 component is entrapped within one nanoparticle. Furthermore, taking a look at the structure of the nanoparticles, cryo-TEM images reveal both lipoplex and spherical particles for *m*LNP-HDR and *p*LNP-HDR (Fig. 1B). Self-assembly particles have been previously studied by Ianiro *et al* to be in an equilibrium between lipoplexes and spheres. [33] In comparison to cryo-TEM images of LNPs with HDR template less lipoplex formation are detected in formulations without HDR template. This might suggest that in the presence of an HDR template sub-complexes between lipids and HDR template are formed. At closer look, cryo-TEM images of *p*LNP-HDR also reveal darker, hence denser, structures, which might be RNP aggregates. [34] *p*LNP-HDR particles were found to start aggregating and sediment over time or at higher concentrations within the *in vivo* study as shown in Supplementary Fig. 5 and 10.

It is of great importance to note that all mice treated with *p*LNP unexpectedly died within 20 h after tail-vein injections while *m*LNP-treated mice remained alive and showed no effects to their well-being. Death of mice may have been due to particle aggregates. *p*LNP were discovered to aggregate and sediment at these higher concentrations (RNP = 15 μM) shown in Supplementary Fig. 10A. Together with the gel retardation assay on protection from degrading enzymes and cryo-TEM images revealing darker spheres for *p*LNP-HDR, LNPs entrapping Cas9-RNP deem less stable than mRNA Cas9-loaded nanoparticles, possibly due to coating of Cas9-RNP on the surface of LNPs (Fig. 1). Another reason for death of mice could be contaminations of Cas9 protein with endotoxins. Cas9 protein was produced in LPS-free ClearColi™ BL21 strain, however during purification contaminations might have been introduced which was not assessed in this study. It has been reported that young mice (7–9) weeks have a LD50 (50 % lethal dose) of 601 Âμg per mouse resulting in lethality due to high levels of IL-10. [35] In contrast, *m*LNP interestingly lead to higher expression of inflammatory cytokines *in vitro* than LNPs containing Cas9-RNP (Fig. 2F).

The differences in particle aggregates and general particle size can explain the observed uptake of *p*LNP in tissue and cell subsets. Alongside high uptake in the liver, *p*LNP was highly retained in the lungs and spleen (Fig. 3B,C). The data shown here supports that aggregating particles are known to be taken up by the lungs as uptake was especially high for *p*LNP. [36] Uptake by the lung could also be due to incorporation of DOTAP in LNPs, as shown by Cheng et al that cationic lipids selectively sort particles to lungs. However, ideal molar percentage of DOTAP for delivery to the lungs was found to be at least 50 % and in this study DOTAP composition was set to a mol% of 0.25 %. [37].

LNPs have been characterized in previous studies to migrate to the liver after intravenous injections due to protein corona formation consisting of mainly apolipoprotein E. [38,39] Incubating *m*LNP and *p*LNP with 50 % serum showed increase in size of nanoparticles suggesting an accumulation of serum proteins on the surface of particles (Supplementary Fig. 10B). Therefore, single cell flow cytometry was performed in this study to investigate both distribution of Cy5.5-sgTOM and gene knock-out efficiencies in liver cell subsets. Herein, Cy5.5-sgTOM via both *p*LNP and *m*LNP was found back in the same cell subsets: mainly LSECs followed by dendritic cells and hepatocytes. *m*LNP-delivered Cy5.5-sgTOM showed higher uptake in hepatocytes than *p*LNPs (Fig. 3D). However, total fluorescent signal of Cy5.5-sgTOM was stronger in the organs of mice treated with *p*LNP, despite similar fluorescent signal within injected formulations (Supplementary Fig. 9), suggesting premature degradation or clearance of sgRNA in non-complexed form. Noteworthily, gene knock-out mediated through CRISPR-Cas9 delivered via *m*LNP was only detected in hepatocytes (60 %) despite delivery of Cy5.5-sgTOM to other cell subsets via single cell flow cytometry. Further validation methods and investigation on gene editing efficiencies in other organs of treated mice are still required.

Moreover, *m*LNP-HDR surpass *p*LNP-HDR in gene editing efficiencies *in vitro* on both reporter HEK293T and HEPA1-6 cells (Fig. 2). Gene editing efficiencies were generally higher on HEK293T cells than on hepatoma cells (Fig. 2A,B). Perhaps internalization of lipid nanoparticles is less efficient in HEPA1-6 cells *in vitro*, an indication for that also being higher cytocompatibility of particles with hepatoma cells (Supplementary Fig. 4C) and internalization resulting in gene knock-out confirmed in hepatocytes in Ai9 mice (Fig. 3 E,F). Further studies such as uptake of fluorescently labelled lipids within LNPs could help investigate internalization and difference between the formulations. On the other hand, gene editing is dependent on cell-cycle and cell differentiation. Cells in a prolonged G1 phase have been shown to favor NHEJ over HDR as HDR only occurs during S/G2 phase. [40,41] HEK293T cells have been studied to induce higher HDR efficiencies than other cell lines such as HeLa and iPSCs. [42] Remarkably, onset of gene correction occurred earlier in cells treated with *m*LNP-HDR despite Cas9 protein localizing significantly later in the nucleus (Fig. 2.C,E). While onset of

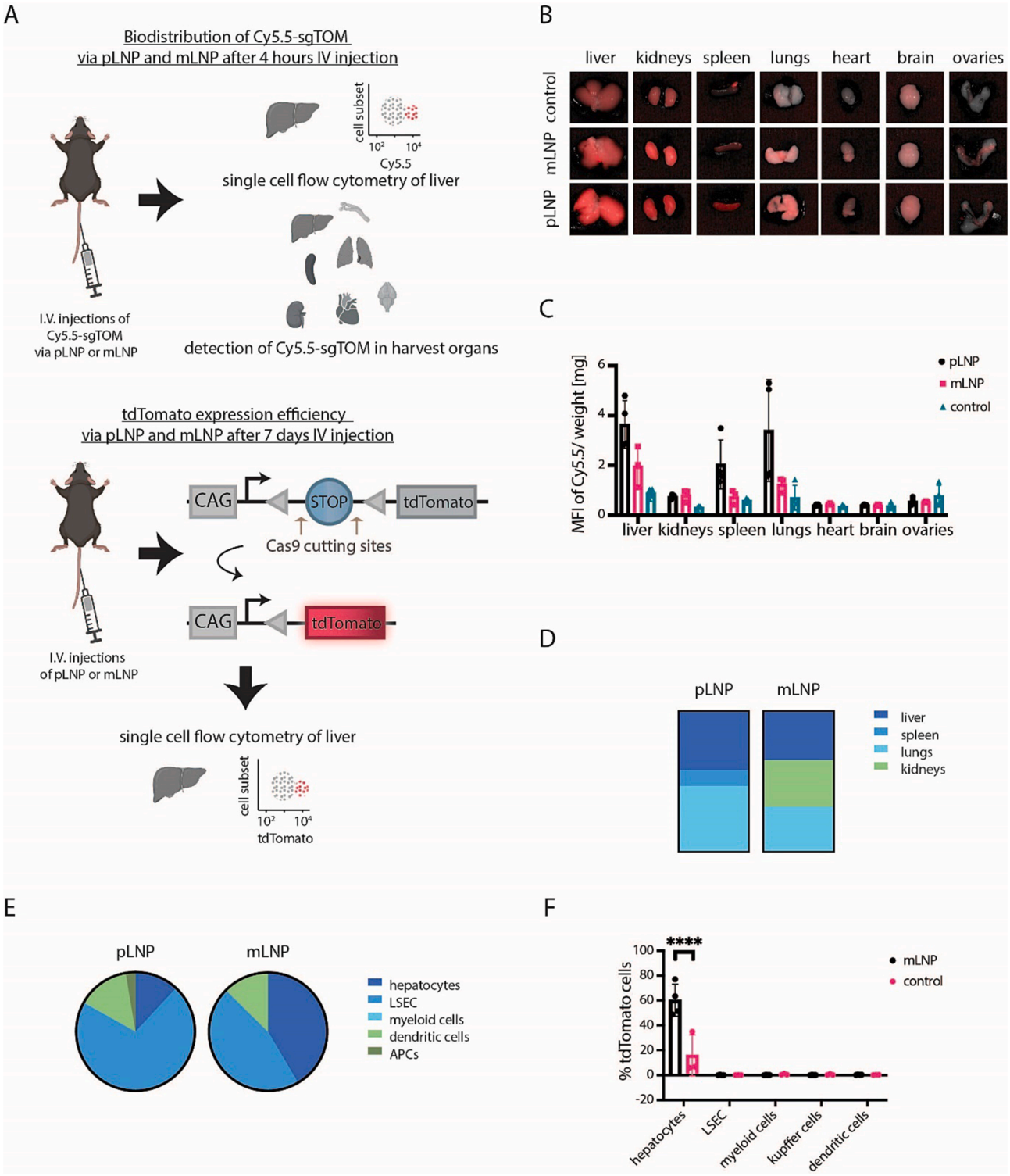

Fig. 3. Biodistribution of Cy5-5-sgTOM and gene editing efficiencies of *p*LNP and *m*LNP *in vivo*. A) Schematic representation of biodistribution and functionality studies of *p*LNP and *m*LNP in Ai9 female mice. Scheme was partially created with Biorender.com. **B)** Images taken with Pearl Impulse Imager of organs harvested from mice treated with *p*LNP and *m*LNP and control LNP. **C)** Biodistribution of Cy5.5-sgTOM after 4 h IV injection of *p*LNP and *m*LNP plotted as MFI per weight of organ. MFI was determined by drawing area of interest around scanned image of organs with Image Studio Lite Software. 4 mice for pLNP, 3 mice for mLNP (as one injection was not successful), 4 mice for control. **D)** Relative distribution of Cy5.5-sgTOM per mice (MFI for each organ divided by cumulative MFI of all organs). Percentage of Cy5.5-sgTOM in mouse organs treated with *p*LNP: 42 % liver, 46 % lungs, 11 % spleen and *m*LNP: 35 % liver, 33 % kidney, 32 % lungs. 4 mice per experimental group (3 mice for *m*LNP as one injection was not successful). **E)** Distribution of Cy5.5-sgTOM in cell subsets of liver in mice treated with *p*LNP or *m*LNP by single cell flow cytometry. Gating strategies and markers defining each cell subset are shown in Supplementary Fig. 11 and table 3, respectively. Percentage of Cy5.5-sgTOM in individual liver cell subsets of the entire signal: *p*LNP: 12 % - hepatocytes, 71 % -LSEC, 0.11 % myeloid cells, 14 % - dendritic cells, 2.66 % APCs and *m*LNP: 41 % - hepatocytes, 46 % - LSEC, 13 % dendritic cells. 4 mice per experimental group (3 mice for *m*LNP as one injection was not successful). **F)** Gene knock-out efficiency given as percentage of tdTomato-positive cells in cell subsets in liver of four mice treated with *m*LNP and three untreated mice (control). Two-way ANOVA was performed via GraphPad Prism 9 (version 9.0) (p-value **** < 0.0001). Gating strategies are shown in Supplementary Fig. 12.

gene correction only starts around 24 h after transfection with *p*LNP-HDR, eGFP positive cells (HDR) were detected after 22 h after treatment with *m*LNP-HDR (Fig. 2E). Moreover, while cells treated with *m*LNP-HDR plateau in HDR around 30 h, HDR in cells treated with *p*LNP-HDR was found to still increase up until the end of the experiment. This may indicate that mRNA delivery results in a higher amount of Cas9 protein at a faster rate. [43] It would be interesting to determine the amount of protein present in cells at various timepoints of gene editing. Another observation is that despite Cas9 being present in the nucleus within a few hours, detection of eGFP in HDR Stoplight reporter cells is only 20 h later (Fig. 2C,E). However, fluorescent proteins have a long half-life probably delaying the detection of eGFP. Studies such as TIDE-R could help determine the exact time of gene correction. The finding of a later onset of gene correction after delivery of the Cas9-RNP could nonetheless be relevant for ongoing studies to optimize the ratio HDR to NHEJ through chemical or genetic disruption of the NHEJ pathway[44].

In conclusion, this study investigated the delivery of CRISPR-Cas9 via lipid nanoparticles as mRNA Cas9 versus Cas9-RNP for gene editing *in vitro* and *in vivo*. Ongoing studies on design of delivery vehicles for CRISPR-Cas9 focus on either cargo format and a comparative analysis of mRNA Cas9 vs RNP has not been studied. Under tested conditions in our study, we conclude that mRNA Cas9 seems a better cargo format for delivery of CRISPR-Cas9 for gene editing via LNPs, resulting not only smaller sized nanoparticles but also in higher gene editing *in vitro* and delivery of functional CRISPR-Cas9 to hepatocytes *in vivo*.

CRediT authorship contribution statement

Johanna Walther: Conceptualization, Data curation, Formal analysis, Writing – original draft, Writing – review & editing. **Deja Porenta:** Formal analysis, Methodology. **Danny Wilbie:** Formal analysis, Methodology. **Cornelis Seinen:** Formal analysis. **Naomi Benne:** Formal analysis, Supervision, Writing – review & editing. **Qiangbing Yang:** Formal analysis, Methodology. **Olivier Gerrit de Jong:** Conceptualization, Supervision, Writing – review & editing. **Zhiyong Lei:** Formal analysis, Investigation, Methodology, Supervision, Writing – review & editing. **Enrico Mastrobattista:** Conceptualization, Funding acquisition, Supervision, Writing – review & editing.

Declaration of competing interest

The authors declare that they have no known competing financial interests or personal relationships that could have appeared to influence the work reported in this paper.

Data availability

Data will be made available on request.

Acknowledgements

We would like to acknowledge Omina Elsharkasy for helping us with cell sorting to select high-expressing eGFP Hepa 1-6 cells. We are grateful to dr. Sander A.A. Kooijmans for the help with setting up the protocol for single cell flow cytometry of liver cells. This research was funded by the Netherlands Organization for Scientific Research (NWO) Talent Program VICI, grant number 865.17.005.

Appendix A. Supplementary data

Supplementary data to this article can be found online at https://doi.org/10.1016/j.ejpb.2024.114207.

References

[1] M. Jinek, et al., A Programmable Dual-RNA – guided, Sci. 1979 (337) (2012) 816–822.
[2] Gasiunas, G., Barrangou, R., Horvath, P. & Siksnys, V. Cas9-crRNA ribonucleoprotein complex mediates specific DNA cleavage for adaptive immunity in bacteria. *Proceedings of the National Academy of Sciences of the United States of America* **109**, 2579–2586 (2012).
[3] M. Zaboikin, T. Zaboikina, C. Freter, N. Srinivasakumar, Non-homologous end joining and homology directed DNA repair frequency of double-stranded breaks introduced by genome editing reagents, PLoS One 12 (2017).
[4] H. Cheng, F. Zhang, Y. Ding, Crispr/cas9 delivery system engineering for genome editing in therapeutic applications, Pharmaceutics. 13 (2021) 1–23.
[5] M. Asmamaw Mengstie, Viral Vectors for the in Vivo Delivery of CRISPR Components: Advances and Challenges, Front. Bioeng. Biotechnol. 10 (2022) 1–6.
[6] X. Hou, T. Zaks, R. Langer, Y. Dong, Lipid nanoparticles for mRNA delivery, Nat Rev Mater. 6 (2021) 1078–1094.
[7] S.C. Semple, et al., Rational design of cationic lipids for siRNA delivery, Nat. Biotechnol. 28 (2010) 172–176.
[8] K.T. Love, et al., Lipid-like materials for low-dose, in vivo gene silencing, Proc Natl Acad Sci U S A 107 (2010) 1864–1869.
[9] J.D. Gillmore, et al., CRISPR-Cas9 In Vivo gene editing for transthyretin amyloidosis, N. Engl. J. Med. 385 (2021) 493–502.
[10] J. Walther, et al., Impact of formulation conditions on lipid nanoparticle characteristics and functional delivery of CRISPR RNP for gene knock-out and correction, Pharmaceutics. 14 (2022).
[11] T. Wei, Q. Cheng, Y.L. Min, E.N. Olson, D.J. Siegwart, Systemic nanoparticle delivery of CRISPR-Cas9 ribonucleoproteins for effective tissue specific genome editing, Nat Commun. 11 (2020) 1–12.
[12] J. Yi, et al., Co-delivery of Cas9 mRNA and guide RNAs edits hepatitis B virus episomal and integration DNA in mouse and tree shrew models, Antiviral Res. 215 (2023) 105618.
[13] Y. Suzuki, et al., Lipid nanoparticles loaded with ribonucleoprotein–oligonucleotide complexes synthesized using a microfluidic device exhibit robust genome editing and hepatitis B virus inhibition, J. Control. Release. 330 (2021) 61–71.
[14] F. Chen, M. Alphonse, Q. Liu, Strategies for nonviral nanoparticle-based delivery of CRISPR/Cas9 therapeutics, Wiley Interdiscip. Rev. Nanomed. Nanobiotechnol. 12 (2020) 1–14.
[15] Y. Lin, E. Wagner, U. Lächelt, Non-viral delivery of the CRISPR/Cas system: DNA versus RNA versus RNP, Biomater. Sci. 10 (2022) 1166–1192.
[16] M.P. Lokugamage, et al., Mild innate immune activation overrides efficient nanoparticle-mediated RNA delivery, Adv. Mater. 32 (2020) 1–9.
[17] S. Vaidyanathan, et al., Uridine depletion and chemical modification increase Cas9 mRNA activity and reduce immunogenicity without HPLC purification, Mol. Ther. Nucleic Acids 12 (2018) 530–542.
[18] S.H. Boo, Y.K. Kim, The emerging role of RNA modifications in the regulation of mRNA stability, Exp. Mol. Med. 52 (2020) 400–408.
[19] E. Kouranova, et al., CRISPRs for optimal targeting: delivery of CRISPR components as DNA, RNA, and protein into cultured cells and single-cell embryos, Hum Gene Ther 27 (2016) 464–475.
[20] S. Liu, et al., Membrane-destabilizing ionizable phospholipids for organ-selective mRNA delivery and CRISPR–Cas gene editing, Nat. Mater. 20 (2021).
[21] S. Lin, B.T. Staahl, R.K. Alla, J.A. Doudna, Enhanced homology-directed human genome engineering by controlled timing of CRISPR/Cas9 delivery, Elife 3 (2014) e04766.
[22] H. Ma, et al., CRI SPR-Cas9 nuclear dynamics and target recognition in living cells, J. Cell Biol. 214 (2016) 529–537.
[23] Y. Lim, et al., Structural roles of guide RNAs in the nuclease activity of Cas9 endonuclease, Nat. Commun. 7 (2016) 1–8.
[24] G. Chen, et al., A biodegradable nanocapsule delivers a Cas9 ribonucleoprotein complex for in vivo genome editing, Nat Nanotechnol 14 (2019) 974–980.
[25] O.F. Khan, et al., Ionizable amphiphilic dendrimer-based nanomaterials with alkyl-chain-substituted amines for tunable sirna delivery to the liver endothelium in vivo, Angewandte Chemie - International Edition 53 (2014) 14397–14401.
[26] C.T. Charlesworth, et al., Identification of preexisting adaptive immunity to Cas9 proteins in humans, Nat Med 25 (2019) 249–254.
[27] A. Li, et al., AAV-CRISPR gene editing is negated by pre-existing immunity to Cas9, Mol. Ther. 28 (2020) 1432–1441.
[28] L. Warren, et al., Highly efficient reprogramming to pluripotency and directed differentiation of human cells with synthetic modified mRNA, Cell Stem Cell 7 (2010) 618–630.
[29] I. Kogut, et al., High-efficiency RNA-based reprogramming of human primary fibroblasts, Nat. Commun. 9 (2018).
[30] M Öktem, E Mastrobattista, OG de Jong, Amphipathic cell-penetrating peptide-aided delivery of Cas9 RNP for in vitro gene editing and correction, Pharmaceutics 15 (2023), https://doi.org/10.3390/pharmaceutics1510250.
[31] A. Glaser, B. McColl, J. Vadolas, GFP to BFP Conversion: a versatile assay for the quantification of CRISPR/Cas9-mediated genome editing, Mol. Ther. Nucleic Acids 5 (2016) e334.
[32] D.T. Braake, N. Benne, C.Y.J. Lau, E. Mastrobattista, F. Broere, Retinoic acid-containing liposomes for the induction of antigen-specific regulatory T cells as a treatment for autoimmune diseases, Pharmaceutics. 13 (2021).
[33] A. Ianiro, et al., Liquid–liquid phase separation during amphiphilic self-assembly, Nat. Chem. 11 (2019) 320–328.

[34] Z. Tan, et al., Block polymer micelles enable CRISPR/Cas9 ribonucleoprotein delivery: physicochemical properties affect packaging mechanisms and gene editing efficiency, Macromolecules. 52 (2019) 8197–8206.
[35] K. Tateda, T. Matsumoto, S. Miyazaki, K. Yamaguchi, Lipopolysaccharide-induced lethality and cytokine production in aged mice, Infect. Immun. 64 (1996) 769–774.
[36] S.Y. Lee, et al., Transient aggregation of chitosan-modified poly(d, l-lactic-co-glycolic) acid nanoparticles in the blood stream and improved lung targeting efficiency, J Colloid Interface Sci. 480 (2016) 102–108.
[37] Q. Cheng, et al., Selective organ targeting (SORT) nanoparticles for tissue-specific mRNA delivery and CRISPR–Cas gene editing, Nat. Nanotechnol. 15 (2020) 313–320.
[38] A. Akinc, et al., Targeted delivery of RNAi therapeutics with endogenous and exogenous ligand-based mechanisms, Mol. Ther. 18 (2010) 1357–1364.
[39] S. Sabnis, et al., A novel amino lipid series for mRNA delivery: improved endosomal escape and sustained pharmacology and safety in Non-human Primates, Mol. Ther. 26 (2018) 1509–1519.
[40] B.T. Dodsworth, K. Hatje, C.A. Meyer, R. Flynn, S.A. Cowley, Rates of homology directed repair of CRISPR-Cas9 induced double strand breaks are lower in naïve compared to primed human pluripotent stem cells, Stem Cell Res. 46 (2020) 101852.
[41] Z. Mao, M. Bozzella, A. Seluanov, V. Gorbunova, DNA repair by nonhomologous end joining and homologous recombination during cell cycle in human cells, Cell Cycle. 7 (2008) 2902–2906.
[42] Y. Miyaoka, et al., Systematic quantification of HDR and NHEJ reveals effects of locus, nuclease, and cell type on genome-editing, Sci. Rep. 6 (2016) 1–12.
[43] B. Schwanhüusser, et al., Global quantification of mammalian gene expression control, Nature. 473 (2011) 337–342.
[44] J. Schimmel, et al., Modulating mutational outcomes and improving precise gene editing at CRISPR-Cas9-induced breaks by chemical inhibition of end-joining pathways, Cell Rep. 42 (2023).